Article

Comparison of Doses in Lunar Habitats Located at the Surface and in Crater

Naser T. Burahmah *[ID] and Lawrence H. Heilbronn [ID]

Nuclear Engineering Department, University of Tennessee, Knoxville, TN 37996, USA; lheilbro@utk.edu
* Correspondence: nburahm1@vols.utk.edu

Abstract: As humanity prepares for extended lunar exploration, understanding the radiation environment on the Moon is important for astronaut safety. This study utilized the Particle and Heavy-Ion Transport code System (PHITS), a stochastic Monte Carlo-based radiation transport code, to simulate the radiation environment inside a habitat, focusing on the impact of galactic cosmic rays (GCRs) interacting with local lunar and habitat material, and to calculate the effective dose equivalent. Placing a lunar base in a crater can provide additional shielding by reducing the GCR flux incident on the base. Furthermore, the secondary radiation field created by GCR interactions may be altered by the local topological features. GCR transport calculations were performed for a hypothetical base on a flat surface and in shallow and deep craters to determine the overall efficacy in dose reduction gained by placing a base in a 100 m diameter crater. Our findings indicate that the depth of lunar habitats significantly influences the effective dose equivalent, with deeper locations offering substantial protection. Specifically, alongside a crater wall at a deep depth (15 m), in solar minimum conditions, the total dose was reduced by approximately 44.9% compared to the dose at the surface. Similarly, at a shallow depth (5 m), a reduction of approximately 10.7% was observed. As the depth of the crater increased, the neutron contribution to the total dose also increased. Comparing the simulated doses to NASA's lifetime exposure limits provides insights into mission planning and astronaut safety, emphasizing the importance of strategic habitat placement and design.

Keywords: lunar radiation; moon; PHITS; lunar missions; GCR

1. Introduction

The return of crewed missions to the Moon this decade is the next step towards the extended human exploration of space, with an emphasis placed on living on lunar and planetary surfaces over long periods of time. For the first time, habitats will be constructed and deployed on those surfaces and will allow long-term stays for crew members. One of the functions of those habitats is to provide some level of protection against the radiation environment of space. This environment consists of galactic cosmic rays (GCRs) and solar energetic particles (SEPs). GCRs are made up of energetic, fully stripped nuclei and electrons, with electrons making up approximately 2% of the total flux and nuclei comprising the other 98% [1]. The nucleonic component of each GCR consists of a stable nucleus, but primarily comprises protons (about 89–90% of the nucleonic component), helium nuclei (about 8–9%), and heavy ions (about 1–2%) [2]. Energies for the nucleonic component run from a few MeV up to several TeV per nucleon, with peak flux values occurring between 300 and 1000 MeV per nucleon. GCRs are present at all times, but their intensities vary with the solar cycle. The maximum GCR flux values occur during the solar minimum, and the minimum GCR flux values occur during the solar maximum. Solar energetic particles are created during solar particle events (SPEs), and as such are sporadic events composed primarily of protons ranging from hundreds of keV to a few GeV, with the majority of the flux being below 10–30 MeV. The flux of protons in the SEP spectrum is greater than the flux of protons from GCRs, and if large enough, can cause debilitating

deterministic effects in crew members if no shielding is provided. However, SEP energies are much lower than GCR proton energies and require much less shielding to protect crew and electronics.

Surface habitats will need to provide adequate shielding such that any exposures during the mission do not exceed the current U.S. National Aeronautics and Space Administration (NASA) lifetime exposure limit of 600 mSv accumulated over all space-related exposures [3]. Much emphasis has been placed on research into the materials that can be used to construct habitats, with several clever designs that use unique composite materials being proposed, as well as the use of the local regolith to augment shielding around the habitat [4,5]. One other consideration for habitat design explored in this paper is whether local topology can be utilized to further reduce the dose inside the habitat. For example, if the habitat is placed in a crater large enough to house the habitat and allow access to it, the crater itself will occlude more of the sky than a habitat placed on a flat surface, thereby reducing GCR and SEP flux incident on the habitat. However, by placing the habitat in a crater or near a crater wall, GCR and SEP interactions in the surrounding regolith will create a flux of secondary light ions and neutrons that can significantly add to the total dose equivalent in the habitat. Slaba et al. [6] studied the point dose equivalent of GCR interactions through varying thicknesses of aluminum and polyethylene, and found that the increase in the dose equivalent beyond 20–30 g cm^{-2} was due to an increase in the secondary light ion and neutron production as the shielding thickness increased. Due to the inherent challenges of obtaining precise measurements on the Moon, simulation codes, such as the PHITS, are employed to emulate the lunar radiation environment. The Monte Carlo code PHITS, in particular, has been utilized in previous studies to analyze the lunar environment [7–11].

On the Moon, secondary albedo neutrons are created by SEP and GCR interactions in the local regolith, and other secondary neutrons are created by interactions among the habitat's materials. Results from recent Chinese rover missions on the Moon indicate that neutrons may comprise up to 20–25% of the dose [12]. The local topology can have a significant impact on the albedo neutron spectrum, altering the number of neutrons as well as potentially altering the neutron energy spectrum. In this paper, we explore how placing a habitat in a shallow crater, a deep crater, and alongside a crater wall affects the effective dose equivalent, and what fraction of that effective dose equivalent comes from protons (both primary and secondary) and neutrons.

2. Materials and Methods

2.1. Simulation Code

In this work, we used the Particle and Heavy-Ion Transport code System (PHITS) version 3.32 as the primary tool to determine the astronaut dose within the lunar environment [13]. The PHITS is a multipurpose Monte Carlo code developed by the Japanese Atomic Energy Agency and several other institutions. The PHITS was employed with Intra-Nuclear Cascade of Liege (INCL4.6) and a jet AA microscopic transport model (JAM) for the nuclear reaction models, using the generalized evaporation model (GEM) for the evaporation model [14–16]. JAERI quantum molecular dynamics (JQMD-2) was enabled to improve the accuracy of the nucleus–nucleus reaction [17]. For low-energy neutron-induced reactions, the code employs Evaluated Nuclear Data libraries. The electron gamma shower (EGS5) algorithm was used to transport electrons, positrons, and photons [18]. For each simulation, 6×10^6 particle histories were utilized. The simulations were performed on an 8-core Windows PC without parallelization. T-track and T-cross tallies were deployed in the calculation. The T-track tally measures the particle fluence within a specified region, while the T-cross tally is used to obtain the current or flux across a specific surface. To determine the effective dose equivalent, the conversion factors embedded in the PHITS for both males and females, as outlined in ICRP Publication 123, were applied under isotropic irradiation (ISO) using the multiplier option [19].

2.2. Geometry

The geometry was a hemisphere recreating a mini moon with a radius of 150 m and a lunar base with a dimension of $10 \times 10 \times 3$ m. Due to computational limitations, the radius of the simulated mini moon was set at 150 m. However, this size was sufficiently large to ensure that all GCRs were in an effective range on the surface. The base was covered with 1 cm thick aluminum as a shielding material against GCRs. The lunar regolith composition implemented in the simulation is presented in Table 1 and is the default composition used in NASA's online radiation transport tool OLTARIS [20]. Five scenarios on the lunar surface were conducted: (1) a base on the lunar surface; (2) a base set in the middle of a shallow (5 m) crater with a radius of 50 m; (3) a base set in the middle of a deep crater (15 m), also with a 50 m radius; (4) a base near the edge of the crater at a shallow depth; and (5) a base near the edge of the crater at a deep depth. An example of the geometry used is shown in Figure 1. The goal of these simulations was to understand the effect of different lunar base placements of for future exploration missions.

Table 1. The elemental composition for the regolith presented in weight fraction.

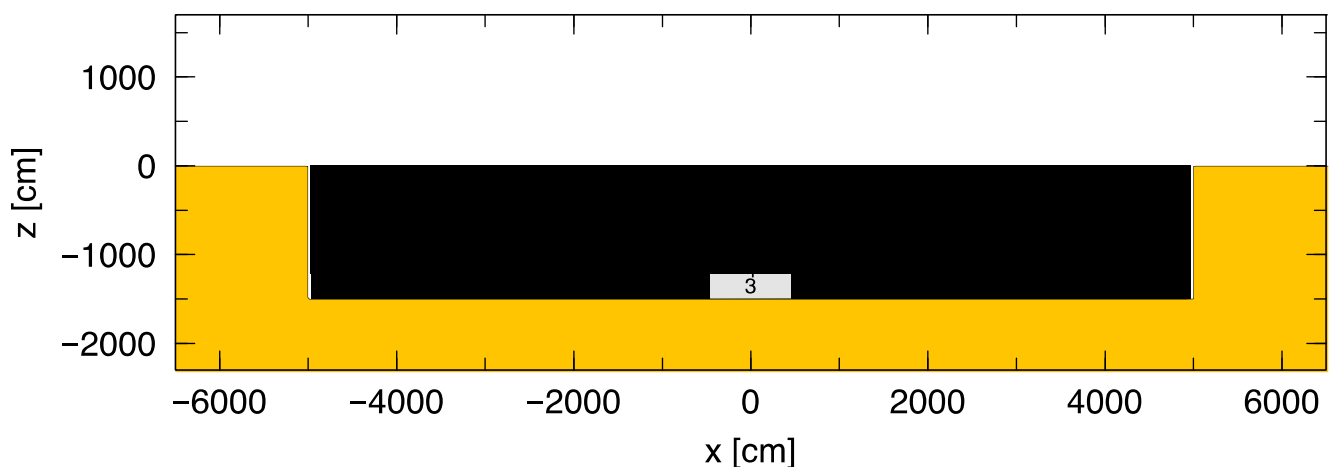| Element	Weight Fraction
O	0.605
Si	0.154
Fe	0.0571
Mg	0.0548
Al	0.0497
Ca	0.0444
Ti	0.0279
Na	0.00286
S	0.000869
Mn	0.000785
Cr	0.00141
K	0.000386
P	0.000229

Figure 1. A representative illustration of the geometry employed in the simulation, showcasing the deep crater scenario, with the yellow color representing the regolith and the silver color in the middle indicating the habitat.

2.3. Radiation Source

After version 3.23, a cosmic-ray source was introduced to the PHITS. GCRs were modeled using the Deutsches Zentrum für Luft- und Raumfahrt (DLR) model [21]. The DLR is referred to as the German Aerospace Center. The source was a spherical source with an isotropic distribution, located inside a sphere with a radius of 150 m, and this

Ssetup was consistent across all simulations. The source projectiles consisted of ions from hydrogen (Z = 1) to iron (Z = 26). Considering the influence of solar activity on cosmic rays, simulations were conducted for both solar minimum and maximum conditions. During a solar minimum, the sun's reduced activity allows a higher flux of cosmic rays, while during a solar maximum, solar activity leads to a decreased GCR flux. The solar modulation potential, represented as 'solarmod' in the PHITS, was set to 0 and 150 to represent solar minimum and maximum conditions, respectively, following the options recommended by the PHITS. The source was an isotropic source distribution inside a sphere with a radius and spherical source of 150 m; this it was consistent across all simulations.

3. Results

The effective dose equivalent values for the different genders, locations, and solar activities are presented in Table 2. These measurements provide insights into the radiation exposure astronauts might encounter in various lunar environments and for each location, offering a comparative perspective on the relative safety of each setting. The dose equivalent is presented in microsieverts per day (μSv d^{-1}) with fractional uncertainty (%). The fractional uncertainty comes from the statistical uncertainty of the sample of source particles. Since no significant differences in the dose between the male and female calculations were observed, the analysis used the male effective dose equivalents to represent the findings. The total effective dose equivalents at the moon surface during the solar minimum and solar maximum were 762.1 μSv d^{-1} and 259.7 μSv d^{-1}, respectively. Figure 2 shows the contribution of protons, neutrons, and other particles to the total dose equivalent.

Table 2. The effective dose equivalent in the various locations and the contribution of each particle to the dose (μSv d^{-1}) and fractional uncertainty (%).

Base Location	Solar Activity	Gender	Proton		Neutron		Total	
			Dose	Uncertainty	Dose	Uncertainty	Dose	Uncertainty
Lunar surface	minimum	Male	230.9	9.6%	120.9	12%	762.1	4.8%
		Female	231	9.6%	121	12%	762.1	4.7%
	maximum	Male	61.4	9.6%	55	10%	260.8	5.6%
		Female	61.4	9.6%	54.7	10.1%	261.1	5.5%
Shallow crater (5 m)	minimum	Male	226.8	11%	119	9.6%	710.7	4.4%
		Female	226.4	11%	118.5	9.6%	711.1	4.4%
	maximum	Male	61.6	9.6%	55	8.4%	247.0	4.1%
		Female	61.4	9.6%	54.7	8.4%	247.1	4.1%
Deep crater (15 m)	minimum	Male	181.9	11%	123.7	9%	619.2	4.6%
		Female	182.8	11%	122.8	9%	619.7	4.6%
	maximum	Male	47.7	10.4%	53.8	8.3%	212.2	4.6%
		Female	47.4	10.4%	53.4	8.3%	212.7	4.6%
Shallow crater edge (5 m)	minimum	Male	230.3	10%	133.3	14%	680.8	5.6%
		Female	230.7	10%	132.5	14%	680.2	5.6%
	maximum	Male	60.4	10.2%	53.2	10.2%	228.2	5.2%
		Female	52.8	10.3%	52.8	10.3%	228.4	5.2%
Deep crater edge (15 m)	minimum	Male	121.6	14.7%	95.7	10.5%	419.8	6.6%
		Female	122.2	14.7%	95	10.6%	420.2	6.6%
	maximum	Male	33.2	14.1%	42.1	8.6%	149.6	6.1%
		Female	33.2	14.2%	41.6	8.7%	149.6	6.1%

Solar minimum on the surface   Solar maximum on the surface
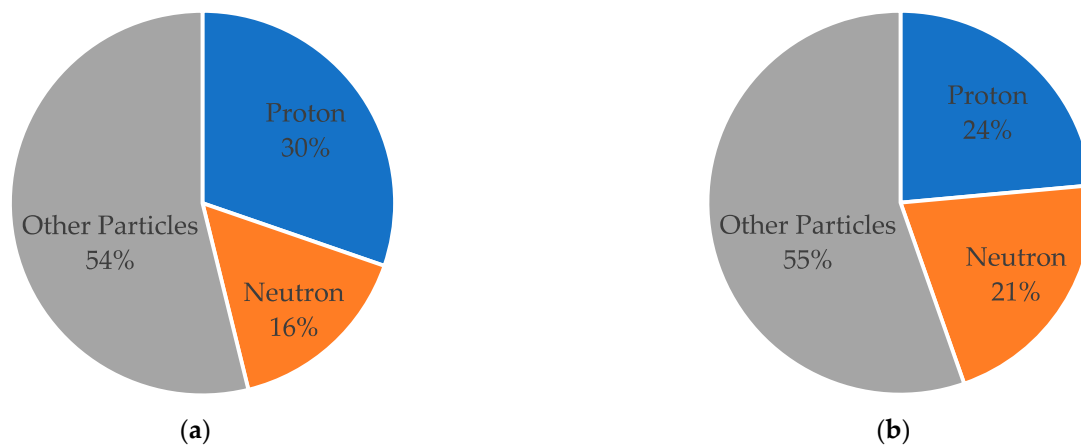

(**a**)   (**b**)

Figure 2. Contribution of protons, neutrons, and other particles to the total dose equivalent on the lunar surface under varying solar activities: (**a**) during solar minimum conditions; (**b**) during solar maximum conditions.

3.1. Solar Minumum

The total dose equivalent on the lunar surface was measured at 762.1 µSv d^{-1}, representing the highest dose across all scenarios presented. Alongside the crater wall at the deep depth (15 m), the total dose equivalent was 419.8 µSv d^{-1}, representing a reduction of approximately 44.9% compared to the dose at the surface. When comparing the dose at the deep depth in the middle of the crater, which was 619.2 µSv d^{-1}, with that alongside the wall, a reduction of 32% was observed.

Similar trends were evident at the shallow depth (5 m). In the middle of the crater, the dose equivalent was 710.7 µSv d^{-1}, while alongside the walls, it was 680.8 µSv d^{-1}. This represents a reduction of approximately 4.2%. Notably, this reduction was not as significant as that observed at a deep depth. The findings suggest a direct correlation between the depth of a crater and the magnitude of dose reduction. Specifically, as the depth increases, there is a noticeable decrease in the total dose equivalent. This reduction is consistent between the crater wall and its center, and has been observed in both shallow and deep simulated locations.

At the surface, the proton and neutron dose equivalent contributions were 30% and 16%, respectively, as shown in Figure 2a.

3.2. Solar Maximum

For the solar maximum, the total dose equivalent on the lunar surface was measured at 260.8 µSv d^{-1}, representing the highest dose across all scenarios presented for this solar activity. Alongside the crater wall at a deep depth, the dose equivalent was 142.4 µSv d^{-1}, marking a 45.4% reduction compared to the surface dose. When comparing the dose equivalent at this depth in the middle of the crater, which was 224.4 µSv d^{-1}, with that alongside the wall, a 36.6% reduction was observed.

Trends similar to those previously observed for the solar minimum were evident at the shallow depth during the solar maximum. In the middle of the crater, the dose equivalent was 247.0 µSv d^{-1}, while it was 228.2 µSv d^{-1} alongside the walls. This represents a reduction of approximately 7.6%. The findings for the solar maximum further reinforce the correlation between the depth of the crater and the magnitude of dose reduction.

From Figure 2b, it can be seen that the contributions of protons and neutrons were approximately 24% and 21%, respectively, in the case of the moon's surface during the solar maximum.

4. Discussion

The amount of GCR flux seen from the base depends on how much of the sky is blocked by local topographical features. On the surface of the Moon, a total solid angle of 2π steradians is visible, whereas a smaller fraction of the sky would be visible from a base surrounded by crater walls. Thus, the effective dose equivalent should decrease as the base moves from a flat surface to inside a crater, as a result of the reduction in the GCR flux incident on the base. Calculations of the solid angle of the sky, as seen from the midpoint of the base, were performed for the base in the center of the crater and the base next to the crater edge for both the shallow and deep crater. Table 3 shows the percent reduction in the GCR flux at those four positions, which is equivalent to the percent reduction in the solid angle seen in those four cases relative to the 2π steradians seen on the surface. Also shown in Table 3 are the percent reductions in the total effective dose equivalent (male, solar minimum and maximum) seen in those four cases relative to the total effective dose equivalent on the surface.

Table 3. The percent reduction in the incident GCR flux, seen at the indicated base locations relative to the flux on the surface along with the calculated percent reduction in the effective dose equivalent at each location relative to the dose on the surface. Calculations shown are for the male effective dose equivalent at the solar minimum and maximum.
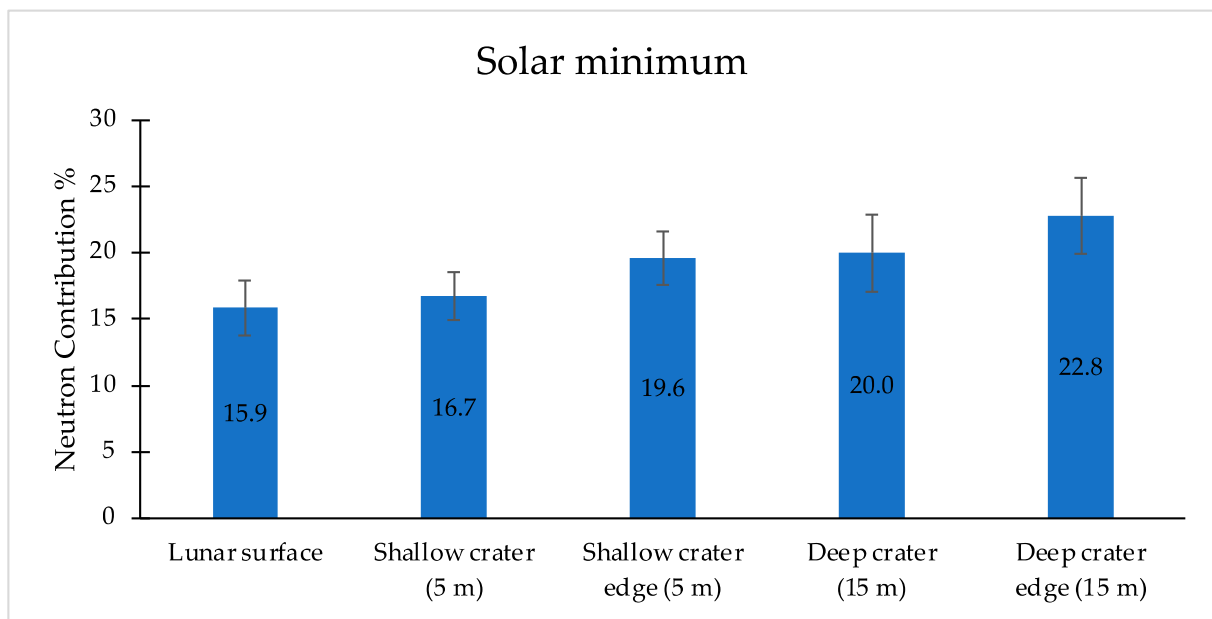
Base Location		Solar Minimum	Solar Maximum
	Percent Reduction in the Incident GCR Flux	Percent Reduction in the Dose in the Base Relative to the Surface Dose	
Shallow center	0.5%	6.7%	5.3%
Shallow crater edge	7.3%	10.7%	12.5%
Deep center	4.2%	18.8%	18.6%
Deep crater edge	25.8%	44.9%	42.7%

Evident in Table 3 is that the decrease in the effective dose equivalent caused by placing a base in a crater is due to more than only a reduction in the incident GCR flux. By placing a base in a position that has additional shielding from local topological features, the nature of the secondary radiation field created by GCR interactions in the local regolith leads to a further reduction in the total effective dose equivalent.
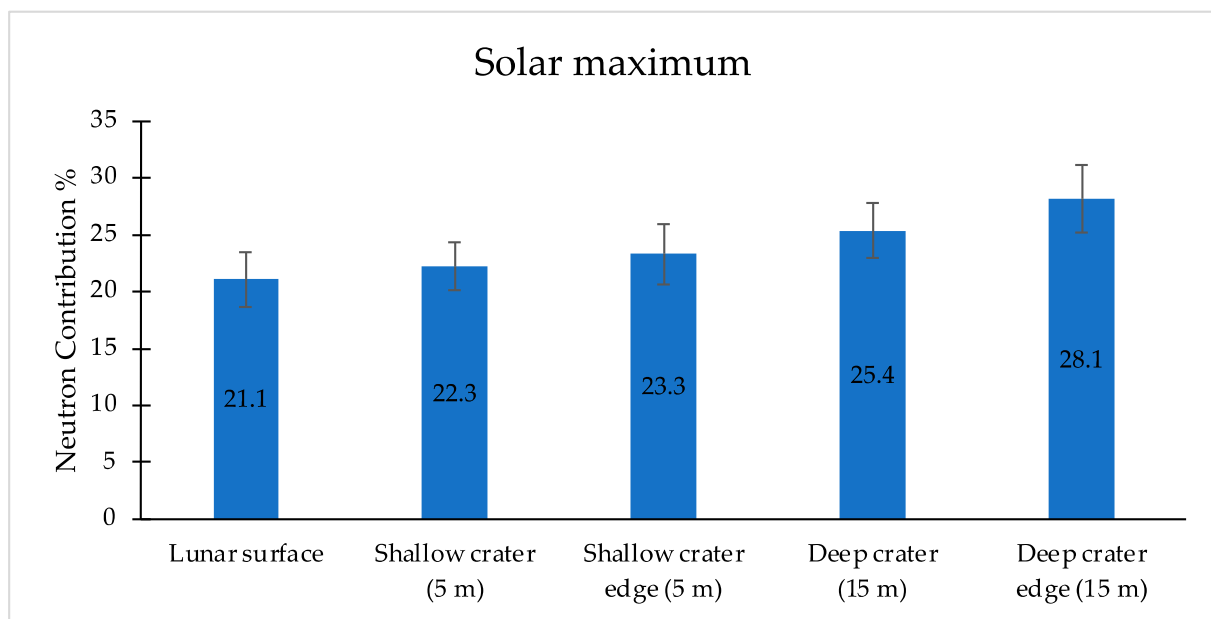
Figure 3 illustrates the neutron contribution to the total dose equivalent by varying the location and solar activity between the solar minimum and maximum. Notably, the neutron contribution increases as the depth of the crater increases. As shown in Figure 3a, the neutron contribution at the moon's surface was 15.9%. However, alongside the deep crater wall, this contribution increased to 22.8%. Moreover, at the same depth, the neutron contribution at the base next to the wall was higher than that in the middle of the crater. The same trends were found in the case of the solar maximum, as shown in Figure 3b.

In a simulated 14-day mission to the moon, the effective dose equivalent on the lunar surface, excluding the dose received during transit to the moon, during the solar minimum was found to be 10.67 mSv, while at the crater edge at a 15 m depth, it was 5.88 mSv. During the solar maximum, the dose equivalent on the lunar surface was 3.65 mSv, and at the crater edge at 15 m, it was 2.02 mSv. For comparison purposes, the annual natural background dose on earth is ~3 mSv.

Comparing the observed doses to NASA's lifetime exposure limit of 600 mSv, during a solar minimum, an astronaut on the lunar surface would reach this limit in approximately 787 days, excluding the dose received during transit to the moon. Table 4 presents the previous NASA career effective dose limits for 1-year missions, targeting a 3% risk of exposure-induced death (REID). The ongoing evolution of standards and limits set by NASA emphasizes the critical importance of continuous monitoring and research in order to ensure astronaut safety.

Figure 3. The neutron contribution of the total dose equivalent at various locations and during different solar activities: (**a**) during solar minimum conditions; (**b**) during solar maximum conditions.

Table 4. Career effective dose limit for 1-year missions for a 3% REID for NASA [22].

Age at Exposure	Effective Dose Limit (mSv)	
	Male	**Female**
30	620	470
35	720	550
40	800	620
45	950	750
50	1150	920
55	1470	1120

5. Conclusions and Future Work

The comprehensive simulations conducted using the PHITS have provided essential insights into the lunar radiation environment. One of the main findings was the significant role of crater depth in mitigating radiation exposure. A habitat next to the wall of a deep crater (15 m) offered a substantial reduction in radiation dose; this was approximately 44.9% less than that experienced on the lunar surface in solar minimum conditions. In addition, the habitat placed alongside a shallow crater wall (5 m) presented a reduction of 10.7%. In contrast, as the depth of the crater increased, the neutron contribution also increased, with the highest contributions reaching approximately 23% and 28% for the solar minimum and maximum, respectively. As we have set our sights on prolonged lunar exploration, it has become evident that a combination of innovative habitat designs, informed by these findings, and the effective utilization of lunar topography will be instrumental in ensuring astronaut safety. Future work will involve testing different regolith compositions, exploring SPEs and examining the dose inside habitats with the same shielding materials, as demonstrated in [23]. Additionally, a comprehensive analysis of the energy spectra of both primary and albedo particles interacting with the lunar base will be conducted at the same locations discussed in this work.

Author Contributions: Conceptualization, N.T.B. and L.H.H.; methodology, N.T.B. and L.H.H.; software, N.T.B. and L.H.H.; writing—original draft preparation, N.T.B. and L.H.H.; writing—review and editing, N.T.B. and L.H.H.; visualization, N.T.B. All authors have read and agreed to the published version of the manuscript.

Data Availability Statement: This study does not report any data.

Conflicts of Interest: The authors declare no conflict of interest.

References

1. National Council on Radiation Protection and Measurement (NCRP). *Guidance on Radiation Received in Space Activities*; NCRP Report No. 98; NCRP: Bethesda, MD, USA, 1988.
2. Simpson, J.A. Elemental and Isotopic Composition of the Galactic Cosmic Rays. *Annu. Rev. Nucl. Part. Sci.* **1983**, *33*, 323–382. [CrossRef]
3. NASA. *Nasa Spaceflight Human-System Standard—Volume 1: Crew Health*; NASA-STD 3001, Revision C; NASA: Washington, DC, USA, 2023.
4. Li, S. Design Structure Matrix Approach Applied to Lunar Habitat Design. *Buildings* **2023**, *13*, 1284. [CrossRef]
5. Rueß, F.; Schänzlin, J.; Benaroya, H. Structural Design of a Lunar Habitat. *J. Aerosp. Eng.* **2006**, *19*, 133–157. [CrossRef]
6. Slaba, T.C.; Bahadori, A.A.; Reddell, B.D.; Singleterry, R.C.; Clowdsley, M.S.; Blattnig, S.R. Optimal shielding thickness for galactic cosmic ray environments. *Life Sci. Space Res.* **2017**, *12*, 1–15. [CrossRef] [PubMed]
7. Zaman, F.A.; Townsend, L.W.; de Wet, W.C.; Burahmah, N.T. The Lunar Radiation Environment: Comparisons between PHITS, HETC-HEDS, and the CRaTER Instrument. *Aerospace* **2021**, *8*, 182. [CrossRef]
8. Zaman, F.A.; Townsend, L.W.; de Wet, W.C.; Looper, M.D.; Brittingham, J.M.; Burahmah, N.T.; Spence, H.E.; Schwadron, N.A.; Smith, S.S. Modeling the Lunar Radiation Environment: A Comparison Among FLUKA, Geant4, HETC-HEDS, MCNP6, and PHITS. *Space Weather* **2022**, *20*, e2021SW002895. [CrossRef]
9. Heilbronn, L.H.; Borak, T.B.; Townsend, L.W.; Tsai, P.-E.; Burnham, C.A.; McBeth, R.A. Neutron yields and effective doses produced by Galactic Cosmic Ray interactions in shielded environments in space. *Life Sci. Space Res.* **2015**, *7*, 90–99. [CrossRef] [PubMed]
10. Bahadori, A.A.; Sato, T.; Slaba, T.C.; Shavers, M.R.; Semones, E.J.; Van Baalen, M.; Bolch, W.E. A comparative study of space radiation organ doses and associated cancer risks using PHITS and HZETRN. *Phys. Med. Biol.* **2013**, *58*, 7183. [CrossRef] [PubMed]
11. Sihver, L.; Sato, T.; Puchalska, M.; Reitz, G. Simulations of the MATROSHKA experiment at the international space station using PHITS. *Radiat. Environ. Biophys.* **2010**, *49*, 351–357. [CrossRef] [PubMed]
12. Zhang, S.; Wimmer-Schweingruber, R.F.; Yu, J.; Wang, C.; Fu, Q.; Zou, Y.; Sun, Y.; Wang, C.; Hou, D.; Böttcher, S.I. First measurements of the radiation dose on the lunar surface. *Sci. Adv.* **2020**, *6*, eaaz1334. [CrossRef] [PubMed]
13. Sato, T.; Iwamoto, Y.; Hashimoto, S.; Ogawa, T.; Furuta, T.; Abe, S.-i.; Kai, T.; Tsai, P.-E.; Matsuda, N.; Iwase, H.; et al. Features of Particle and Heavy Ion Transport code System (PHITS) version 3.02. *J. Nucl. Sci. Technol.* **2018**, *55*, 684–690. [CrossRef]
14. Boudard, A.; Cugnon, J.; David, J.C.; Leray, S.; Mancusi, D. New potentialities of the Liège intranuclear cascade model for reactions induced by nucleons and light charged particles. *Phys. Rev. C* **2013**, *87*, 014606. [CrossRef]

15. Nara, Y.; Otuka, N.; Ohnishi, A.; Niita, K.; Chiba, S. Relativistic nuclear collisions at 10*A* GeV energies from *p* + Be to Au+Au with the hadronic cascade model. *Phys. Rev. C* **1999**, *61*, 024901. [CrossRef]

16. Furihata, S. Statistical analysis of light fragment production from medium energy proton-induced reactions. *Nucl. Instrum. Methods Phys. Res. Sect. B Beam Interact. Mater. At.* **2000**, *171*, 251–258. [CrossRef]

17. Ogawa, T.; Sato, T.; Hashimoto, S.; Satoh, D.; Tsuda, S.; Niita, K. Energy-dependent fragmentation cross sections of relativistic ^{12}C. *Phys. Rev. C* **2015**, *92*, 024614. [CrossRef]

18. Hirayama, H.; Namito, Y.; Nelson, W.R.; Bielajew, A.F.; Wilderman, S.J. *The EGS5 Code System*; United States Department of Energy: Washington, DC, USA, 2005.

19. Dietze, G.; Bartlett, D.T.; Cool, D.A.; Cucinotta, F.A.; Jia, X.; McAulay, I.R.; Pelliccioni, M.; Petrov, V.; Reitz, G.; Sato, T. ICRP Publication 123: Assessment of Radiation Exposure of Astronauts in Space. *Ann. ICRP* **2013**, *42*, 1–339. [CrossRef] [PubMed]

20. Singleterry, R., Jr.; Blattnig, S.; Clowdsley, M.; Qualls, G.; Sandridge, C.; Simonsen, L.; Norbury, J.; Slaba, T.; Walker, S.; Badavi, F. *OLTARIS: On-Line Tool for the Assessment of Radiation in Space (NASA/TP-2010-216722)*; National Aeronautics and Space Administration (NASA): Washington, DC, USA, 2010.

21. Matthiä, D.; Berger, T.; Mrigakshi, A.I.; Reitz, G. A ready-to-use galactic cosmic ray model. *Adv. Space Res.* **2013**, *51*, 329–338. [CrossRef]

22. Cucinotta, F.A. *Radiation Risk Acceptability and Limitations*; Space Radiation Program Element; NASA Johnson Space Center: Houston, TX, USA, 2010.

23. Zaman, F.A.; Townsend, L.W.; Burahmah, N.T. Radiation Risks in a Mission to Mars for a Solar Particle Event Similar to the AD 993/4 Event. *Aerospace* **2021**, *8*, 143. [CrossRef]